

Thermal-Mechanical and Thermodynamic Properties of Graphene Sheets using a Modified Nosé-Hoover Thermostat

Ching-Feng Yu¹, Wen-Hwa Chen^{1,2}, Kun-Ling Chen¹, Hsien-Chie Cheng^{2,3}

Abstract: The investigation assesses the thermal-mechanical and thermodynamic properties of various graphene sheets using a modified Nosé-Hoover (NH) thermostat method incorporated with molecular dynamics (MD) simulation. The investigation begins with an exploration of their thermal-mechanical properties at atmospheric pressure, including Young's modulus, shear modulus, Poisson's ratio, specific heats and linear and volumetric coefficients of thermal expansion (CTE). Two definitions of the line change ratio ($\Delta L/L$) are utilized to determine the linear CTE of graphene sheets, and the calculations are compared with each other and data in the literature. To estimate the volumetric CTE values, the Connolly surface method is applied to predict the volume of the deformed graphene sheets in the free relaxation state and under temperature loading. Their specific heats are also determined by estimating the ratio of the amount of heat energy per unit mass that is required to raise the temperature by one degree. Finally, the dependences of the size and temperature on the thermal-mechanical and thermodynamic properties are examined. The calculations are validated by comparison with the results obtained from the existing thermostats and with the literature experimental and theoretical data. The results indicate that the presently calculated thermal-mechanical and thermodynamic properties of graphene sheets are very similar to the published experimental and theoretical results. The graphene sheets tend to have a negative linear CTE at temperatures below 300 K. Additionally, the calculated linear CTE of graphene sheets depends strongly on the line-change-ratio assumptions. The modified NH thermostat is the only one of five thermostats that can accurately reproduce the Debye T^3 -dependent specific heat at temperatures below the Debye temperature.

¹ Department of Power Mechanical Engineering, National Tsing Hua University, Hsinchu, Taiwan, ROC.

² Corresponding author

³ Department of Aerospace and Systems Engineering Feng Chia University, Taichung, Taiwan, ROC.

Keywords: Thermal-mechanical and thermodynamic properties, Graphene sheet, Modified Nosé-Hoover Thermostat, Molecular dynamics, Temperature dependence

1 Introduction

Graphene sheets, consisting of a single layer of carbon atoms that are arranged in two-dimensional (2D) hexagonal structure, are considered to be a new generation of material owing to its remarkable electrical, mechanical and thermal properties. Accordingly, graphene sheets have various potential applications in several fields, such as fuel cells, nanoelectronics, transistors, sensors, and conduction media in polymer composites [Novoselov, Jiang, Schedin, Booth, Khotkevich, and Morozov (2005); Geim and Novoselov (2007); Mohanty and Berry (2008); Inoue, Kobayashi, Ogata, and Gotoh (2010)]. In particular, graphene sheets are ideal nanofillers for improving the mechanical properties of polymer-based composites because of their excellent Young's modulus and high intrinsic strength [Fukushima and Drzal (2002); Stankovich, Dikin, Dommett, Kohlhaas, Zimney, Stach, Piner, Nguyen, and Ruoff (2006a); Lee, Wei, Kysar, and Hone (2008); Wei, Luo, Fan, Zheng, Yan, Yao, Li, and Zhang (2009); Shi and Zhao (2011)]. Consequently, many relevant investigations have focused on two subjects-the synthesis of the graphene sheets and assessment of their physical properties. For example, [Novoselov, Geim, Morozov, Jiang, Zhang, Dubonos, Grigorieva, and Firsov (2004)] prepared graphene films by the mechanical exfoliation of small mesas of highly oriented pyrolytic graphite. [Meyer, Geim, Katsnelson, Novoselov, Booth, and Roth (2006)] successfully distinguished single- from multi-layered graphene sheets by analyzing electron diffraction patterns. [Stankovich, Piner, SonBinh, and Ruoff (2006b)] developed a novel method for synthesizing and exfoliating the isocyanate-treated graphene oxide nanoplatelets. [Bunch, van der Zande, Verbridge, Frank, Tanenbaum, Parpia, Craighead, and McEuen (2007)] presented an experimental method for suspending single- and multi-layered graphene sheets using electromechanical resonators. [Lee, Wei, Kysar, and Hone (2008)] utilized atomic force microscopy (AFM) to measure the Young's modulus of graphene sheets, finding a result of approximately 1TPa. [Kim, Zhao, Jang, Lee, Kim, Kim, Ahn, Kim, Choi, and Hong (2009)] reported on the direct synthesis of large-scale graphene films using chemical vapor deposition on thin nickel layers, and presented two methods of patterning the films and transferring them to arbitrary substrates. [Popov, Van Doren, and Balkanski (2000)] utilized the lattice dynamical model with Born's perturbation method to determine the Young's modulus of graphene sheets. [Odegard, Gates, Nicholson, and Wise (2002); Li and Chou (2003)] applied the equivalent atomistic continuum model to calculate the mechanical properties of graphene sheets. In the model, the typical elements of structural mechanics, including rods, beams

and shells with appropriate mechanical properties, are used to simulate the static and dynamic behaviors of graphene sheets. [Konstantinova, Dantas, and Barone (2006)] performed *ab initio* calculations using the ABINIT pseudopotential code [Gonze, Beuken, Caracas, Detraux, Funchs, Rignanese, Sindic, Verstraete, Zerah, Jollet, Terrent, Roy, Mikami, Ghoser, Raty, and Allan (2002)] to evaluate the electronic and Young's properties of graphene sheets. [Pozrikidis (2008)] proposed theoretical framework to describe the deformation of graphene sheets using the membrane theory of the shells. [Jiang, Wang, and Li (2009a)] used molecular dynamics (MD) and the intrinsic thermal vibration theorem to calculate the Young's modulus from the thermal mean-square amplitude of vibration at temperatures from 100 K-500 K. [Jiang, Huang, and Hwang (2005)] applied the continuum theories with the local harmonic approximation to determine the Young's modulus, linear coefficient of thermal expansion (CTE) and specific heat (C_v) of graphene sheets. Mounet and Marzari investigated the linear CTE, Young's modulus and C_v of graphene sheets [Mounet and Marzari (2005)] by making density-functional theory total-energy calculations and applying density-functional perturbation theory lattice dynamics within the generalized gradient approximation. [Jiang, Wang, and Li (2009b)] adopted the non-equilibrium Green's function method to evaluate the CTE of single-walled carbon nanotubes and graphene. They found that the CTE of graphene is very sensitive to the substrate. Without a substrate, graphene has a greater span of negative CTE at low temperatures and in addition, holds a very small value at the high temperature limit.

In this study, the effects of chirality, size and temperature on the Young's modulus, shear modulus and Poisson's ratio are firstly examined by performing MD simulation in which a modified Nosé-Hoover (NH) thermostat method is applied [Chen, Wu, and Cheng (2011a); Chen, Wu, and Cheng (2011b); Cheng, Wu, and Chen (2012)]. In the modified NH thermostat method, the phonon effects induced by virtue of the lattice vibrational and zero-point energy are properly considered, yielding an accurate estimate of the quantum effects on the temperature-dependent properties of graphene sheets. Next, the linear and volumetric CTEs of a graphene sheet are investigated as functions of temperature and size. In particular, very few studies have sought to predict the volumetric CTE of a graphene sheet. To the best of the author's knowledge, this investigation is the first to address this issue using the Connolly surface method. Furthermore, the specific heat of graphene sheets against temperature and size is further determined. Finally, the calculations are compared to both theoretical and experimental data concerning the linear and volumetric CTEs, specific heat, Young's modulus, shear modulus, as well as Poisson's ratio.

2 Simulation model and method

In the MD program herein, the covalent bonds, σ -bonds, of carbon atoms are described using the Tersoff-Brenner potential [Erkoc (1997)], which is typically employed in simulations that are carried out for studying graphene sheets, fullerene and CNTs [Chen, Cheng, and Hsu (2007); Cheng, Hsu, and Chen (2009); Cheng, Liu, and Chen (2009); Chen, Wu, and Cheng (2011a); Chen, Wu, and Cheng (2011b); Cheng, Wu, and Chen (2012); Chen, Liu, Wu, and Cheng (2012)]. The Tersoff-Brenner potential is given by,

$$U = f_c(r_{ij}) \{V_R(r_{ij}) - \overline{B}_{ij}V_A(r_{ij})\}, \quad (1)$$

where r_{ij} is the distance between two joining atoms, i and j , as presented in Fig.1. $f_c(r_{ij})$ is the cut-off function of the Tersoff-Brenner potential. The cut-off function is given as follows,

$$f_c(r_{ij}) = \begin{cases} 1 & (r_{ij} < R - D) \\ \frac{1}{2} - \frac{1}{2} \sin \left[\frac{\pi}{2} (r_{ij} - R) / D \right] & (R - D < r_{ij} < R + D) \\ 0 & (r_{ij} > R + D) \end{cases}, \quad (2)$$

where D denotes the half width and R is the cutoff length. In general, the cutoff function is a simple decaying function that outputs the weighting of covalent bonds that are centered at $r_{ij} = R$. If the inter-atomic distance r_{ij} is less than $R - D$, then the potential energy should be considered, and the weighting becomes unity. When the distance is between $R - D$ and $R + D$, the weighting is between 1 and 0. When it exceeds larger than $R + D$, the potential energy can be ignored, and the weighting equals zero. The functions $V_R(r_{ij})$ and $V_A(r_{ij})$ in Eq. (1) represent the short-range pair potentials that describe the repulsive and attractive interactions between atoms i and j . They are given by,

$$V_R(r_{ij}) = \frac{D_e}{S - 1} e^{-\sqrt{2S}\beta(r_{ij} - r_e)}, \quad (3)$$

and

$$V_A(r_{ij}) = \frac{D_e S}{S - 1} e^{-\sqrt{2/S}\beta(r_{ij} - r_e)}. \quad (4)$$

where r_e is the equilibrium distance between two carbon atoms, and D_e, S and β are material-dependent constants. \overline{B}_{ij} in Eq. (1) changes the covalent bonding energy in a way that depends on θ_{jik} , and is specified by $\overline{B}_{ij} = (B_{ij} + B_{ji}) / 2$, where

$$B_{ij} = \left(1 + a^n \left\{ \sum_{k(\neq i, j)} g(\theta_{jik}) \right\}^n \right)^{-\delta}, \quad (5)$$

where

$$g(\theta_{jik}) = 1 + c^2/d^2 - c^2/(d^2 + (h - \cos\theta_{jik})^2), \quad (6)$$

In Eq. (6), a , n , δ , c , d , and h are all material-dependent constants. Table 1 presents the parameters that are used in the Tersoff-Brenner potential for a carbon system [Erkoc (1997)].

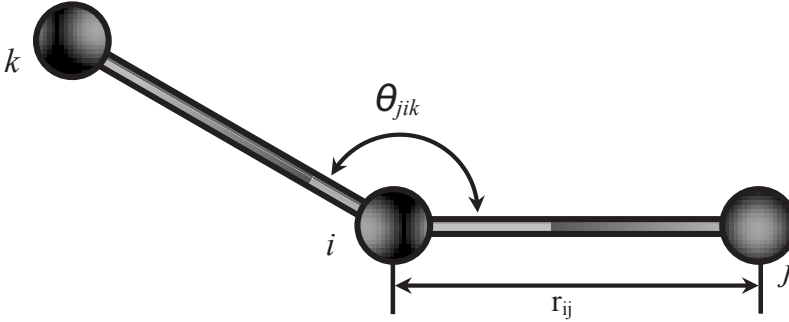


Figure 1: Geometric relationship between covalent bonds

Table 1: Parameters of Tersoff-Brenner potential for graphene sheet

R_u (nm)	0.20
R_b (nm)	0.17
D_e (eV)	6.325
S	1.29
$\beta_{(nm)}^{-1}$	15
Re (nm)	0.1315
a	1.1304×10^{-2}
n	1
δ	0.80469
c	19
d	2.5
h	-1
R (nm)	0.185
D (nm)	0.005

To control the temperature of the system, the modified NH thermostat method presented by [Chen, Wu, and Cheng (2011a)] is applied, which considers the contribu-

tion of phonons by virtue of the vibrational energy of the lattice and the zero-point energy, based on the Debye theory. Essentially, both the kinetic and the potential energies of atoms are taken into account in the calculation of the system temperature. Moreover, this method is more feasible and effective for dealing with a solid molecular system, in which atoms interact with strong forces, especially at temperatures below the Debye temperature. Based on the Debye theory [Debye (1912)], the relationship among the lattice vibrational energy, the zero-point energy and temperature can be expressed as,

$$U(\vec{r}_1, \vec{r}_2, \dots, \vec{r}_N) + \sum_{i=1}^N \frac{\vec{p}_i^2}{2m_i} = U_0 + 3Nk_BTD(x), \quad (7)$$

where $D(x)$ is the Debye function, U_0 is the zero-point energy, and x is a dimensionless temperature parameter that equals $x = \theta_D/T$, where θ_D is the Debye temperature. From Eq. (2-5), the equations of motion are rewritten as,

$$\frac{d\vec{r}_i}{dt} = \frac{\vec{p}_i}{m_i} \quad (i = 1, 2, \dots, N), \quad (8)$$

$$\frac{d\vec{p}_i}{dt} = -\frac{\partial U}{\partial \vec{r}_i} - \vec{p}_i \frac{p_\eta}{Q} \quad (i = 1, 2, \dots, N), \quad (9)$$

$$\frac{d\eta}{dt} = \frac{p_\eta}{Q}, \quad (10)$$

and

$$\frac{dp_\eta}{dt} = 2 \left[U(\vec{r}_1, \vec{r}_2, \dots, \vec{r}_N) - U_0 + \sum_{i=1}^N \frac{\vec{p}_i^2}{2m_i} - 3Nk_BTD(x) \right]. \quad (11)$$

where N is the number of atoms of the system, U stands for the potential energy, \vec{r}_i , \vec{p}_i and m_i are the coordinates, momenta and mass of atom i , η and p_η represent two parameters relative to the additional degree of freedom and its virtual momenta of the external system, k_B is Boltzmann's constant, Q denotes the effective mass of the external system and T is the externally set temperature. The methods have been successfully tested on different gold nanocrystals to characterize their melting point and constant volume specific heat, and also their size and temperature dependence [Chen, Wu, and Cheng (2011a)], on carbon fullerenes to explore their linear and volumetric CTEs at temperatures below Debye temperature and phase transformation behaviors at atmospheric pressure [Chen, Wu, and Cheng (2011b)], and on short single-walled carbon nanotubes to predict their low temperature thermal conductivities and also their length, diameter and chirality dependences [Cheng,

Wu, and Chen (2012)] and the temperature-dependent vibrational behaviors and dynamic Young's modulus [Chen, Liu, Wu and Cheng (2012)].

In the study, an example of graphene atomistic structure for MD simulation is demonstrated in Fig. 2. All the graphene sheets under the present investigation are square in shape (i.e., $L_x = L_y = L$), in which L is in the range of 20 to 50 Å. To determine the Young's modulus, the atoms on the bottom surface of the graphene sheet are fully constrained (red zone in Fig. 2) while a vertical displacement is applied to those on the top surface (blue zone in Fig. 2). The Young's modulus can be obtained using the following equation,

$$E = \frac{1}{V} \frac{\partial^2 U}{\partial^2 \varepsilon}, \quad (12)$$

where E is Young's modulus; V is the volume of the graphene sheet and ε is tensile strain. The strain energy U of the graphene sheet is calculated by strain ε resulting from changing the displacement of the atoms on the top surface. By the $U - \varepsilon$ relation obtained from curve-fitting analysis, the second derivative of the strain energy with respect to the strain yields the Young's modulus according to Eq. (12). In addition, the Poisson's ratio, defined as the ratio of the transverse contraction strain to the longitudinal extension strain in the stretching direction, can be expressed as,

$$\nu = -\frac{\varepsilon_t}{\varepsilon_l}, \quad (13)$$

where ε_t and ε_l are the strains that are measured in the direction of contraction and stretching, respectively. To compute the shear modulus, shear loading is applied. The atoms on the bottom surface of the graphene sheet are constrained (red zone in Fig. 2), and a horizontal displacement is applied to those on the top surface (blue zone in Fig. 2). By following the same derivation procedure as the Young's modulus, the shear modulus can be obtained using the following equation,

$$G = \frac{1}{V} \frac{\partial^2 U}{\partial^2 \gamma}, \quad (14)$$

where γ represents the shear strain.

The linear and volumetric CTEs of a graphene sheet can be defined as the first derivative of the line (volume) change ratio with respect to temperature,

$$\alpha_L = \frac{1}{L_0} \left(\frac{\partial L}{\partial T} \right), \quad (15)$$

and

$$\alpha_V = \frac{1}{V_0} \left(\frac{\partial V}{\partial T} \right). \quad (16)$$

where L_0 is the length of the graphene sheet at zero temperature and V is the volume of the graphene sheet at zero temperature. Finally, heat capacity C_v is defined as the required heat to raise the unit mass of a substance by one degree and can be expressed as

$$C_v = \frac{1}{m} \left(\frac{\partial Q}{\partial T} \right)_v, \quad (17)$$

where m is the mass of the graphene sheet, and Q denotes amount of heat.

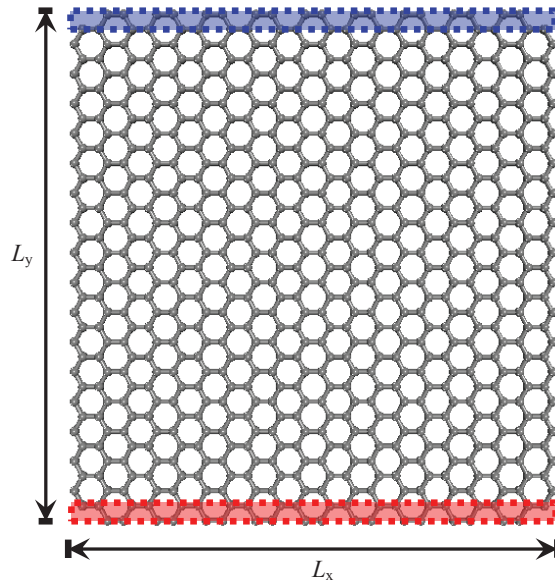


Figure 2: Schematic graphene sheet under tensile displacement

3 Results and discussion

In the MD simulation, a time step of $\Delta t = 5 \times 10^{-16}$ s is used and the number of equilibrating time steps is 10^6 . A random sampling method is performed to take a sample out of every 1,000 time steps from 2×10^6 time steps. In addition to the modified NH thermostat, the standard NH [Nosé (1984); Hoover (1985)], Nosé-Hoover chain (NHC) [Martyna, Tuckerman, and Klein (1992)], “massive” NHC (MNHC) [Martyna, Tuckerman, and Klein (1992)] and velocity-rescaling [Woodcock (1971)] thermostat are also applied to investigate the temperature-dependent linear and volume CTEs of graphene sheets.

3.1 Young's modulus of graphene sheets

Figures 3 and 4 present the Young's moduli of zigzag and armchair types of graphene sheets as functions of temperature for various side lengths (L) of the square graphene sheets. It is found that the Young's moduli of the zigzag and armchair types of graphene sheets decline as the temperature increases. The rates of decrease for the zigzag and armchair graphene sheets are around 3.8 and 3.3%, respectively, which could, by no means, be considered significant. In addition, the reason for the dependence is due to that temperature would weaken interatomic bonds among Carbon atoms in a graphene sheet, thereby leading to a reduced strength. Moreover, the Young's moduli of the zigzag and armchair graphene sheets seem also to fall as the side lengths increases. At 300 K, the Young's modulus of the zigzag graphene sheet varies from 990 to 960 GPa as the side length increases from 20 to 50 Å, whereas that of the armchair sheet varies from 1130 to 1020 GPa.

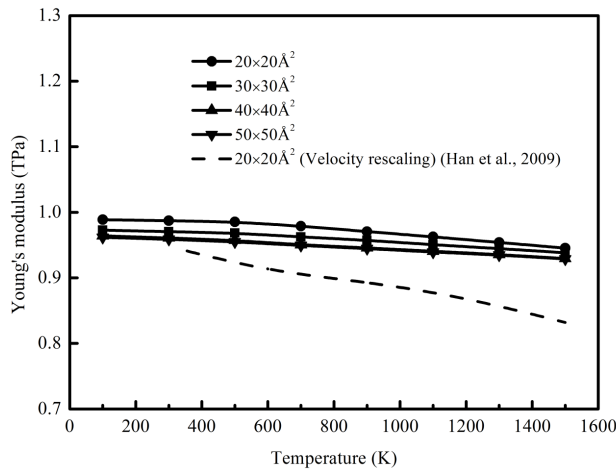


Figure 3: Young's modulus of zigzag graphene sheet as a function of temperature for various side lengths

Evidently, size has an adequate effect on the Young's modulus of the graphene sheet. Accordingly, the decrease rates for the size effect for the zigzag and armchair graphene sheets are around 3.0 and 9.7%, respectively. It is clear that the size effect for the armchair graphene sheet would be considerably larger than that for the zigzag graphene sheet. The fair dependence on size is probably attributable to the surface effects of nanostructures, which are composed of the effects of surface energy [Dingreville and Qu (2005)], surface stress [Cammarata and Sieradzki (1989)] and surface relaxation [Guo and Zhao (2005)]. These effects depend strongly on

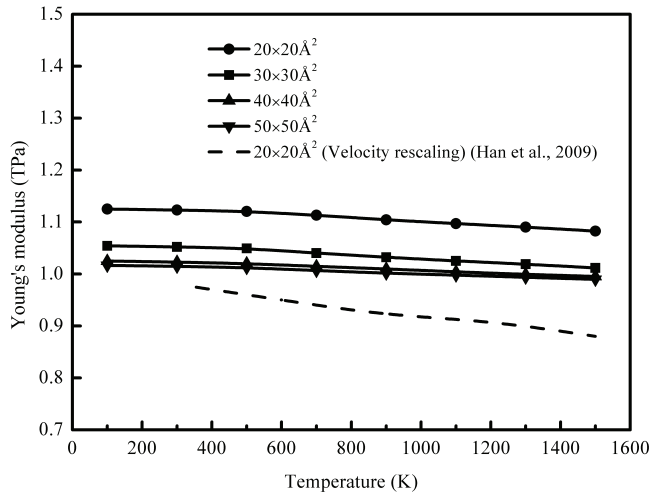


Figure 4: Young's modulus of armchair graphene sheet as a function of temperature for various side lengths

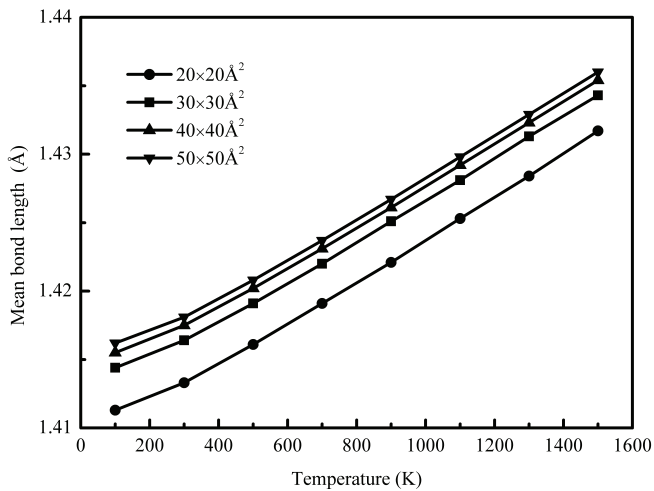


Figure 5: Mean bond length of graphene sheet as a function of temperature

the surface to volume ratio. For nano-size particles, wires and films, the surface to volume ratio becomes significant, and so does the surface or boundary effects. Additionally, the effect of size on the Young's modulus of a graphene sheet can be elucidated by determining the mean bond length of a graphene sheet as a function of temperature at various side lengths, as displayed in Fig. 5. The mean bond length clearly decreases as the temperature and side length increase. As the bond length increases, the intermolecular interactions become weaker, thereby reducing the Young's modulus.

Finally, once the side length reaches approximately 40 Å, the Young's moduli of both the zigzag and armchair graphene sheets tend to be stable. The Young's moduli of the zigzag and armchair graphene sheets at 300 K converge to around 960 and 1010 GPa, respectively. Notably, the Young's modulus of the armchair graphene sheet is larger than that of the zigzag graphene sheet by about 50 GPa. The present results are further compared to the theoretical data of [Han, He, and Zheng (2009)] using the velocity-rescaling thermostat incorporated with MD simulation, as also shown in Figs. 3 and 4. Their simulation results also present a similar temperature dependence: the Young's modulus decreases with temperature. By comparing the results of the graphene sheet size $20 \times 20 \text{ \AA}^2$, a considerable difference can be observed between the present calculations and those of [Han, He, and Zheng (2009)]. And, Ref. [Han, He, and Zheng (2009)] using the velocity-rescaling thermostat would yield a much smaller Young's modulus across the temperature span than the present calculations. This may be due to its lack of account of phonon effect and so quantum effect [Chen, Wu, and Cheng (2011a)].

3.2 Shear modulus of graphene sheet

The shear moduli of the zigzag and armchair graphene sheets are shown in Fig. 6 and 7. Like the Young's moduli, temperature and size can also degrade the shear moduli, and the decrease rate is about 5.2% for the zigzag one and approximately 4.2% for the armchair one as the temperature increases from 100 to 1500K. Furthermore, at 300K, the shear modulus of the zigzag graphene sheets decreases from 250 to 210 GPa as the side length increases from 20 to 50 Å while that of the armchair sheet falls from 310 to 280 GPa, which also indicates that the armchair graphene sheets tend to be stiffer than the zigzag. The decrease rates of the shear moduli of the zigzag and armchair graphene sheets with temperature are around 16.0 and 9.6%, respectively. Notably, the shear moduli of these two types of graphene sheets would all approach a converged limit, i.e., 210 GPa for the zigzag one and 280 GPa for the armchair at 300K, as the side length exceeds 40 Å. The limit can be regarded as the bulk shear modulus of the graphene sheets. Besides, it is not difficult to find that size would have a greater effect on the shear

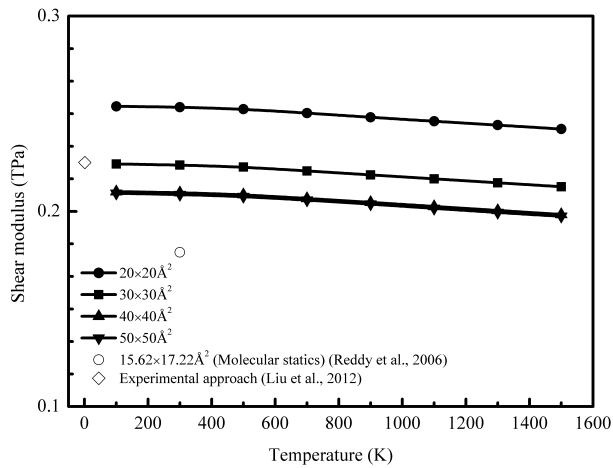


Figure 6: Shear modulus of zigzag graphene sheet as a function of temperature for various side lengths

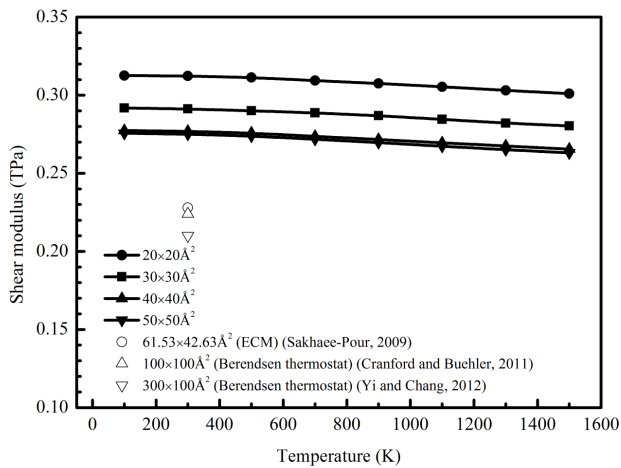


Figure 7: Shear modulus of armchair graphene sheet as a function of temperature for various side lengths

modulus of the graphene sheets than temperature. Finally, the present calculations are further compared to the published theoretical [Reddy, Rajendran, and Liew (2006); Yi and Chang (2012)] and experimental results [Liu, Metcalf, Robinson, Houston, and Scarpa (2012)], which are also shown in Figs 6 and 7. It is worth noting that the present shear modulus of the zigzag graphene sheets at around 0K is consistent with the experimental data of [Liu, Metcalf, Robinson, Houston, and Scarpa (2012)]. The published theoretical data applied include [Reddy, Rajendran, and Liew (2006)] using molecular statics for the zigzag graphene sheets and for the armchair ones, [Sakhaee-Pour (2009)] using an equivalent continuum modeling (ECM) technique and [Cranford and Buehler (2011)]; Yi and Chang (2012)] both using the Berendsen thermostat incorporated with MD simulation. Again, it should be also noted that not only the molecular statics but also the ECM approach and the MD simulation using the Berendsen thermostat are incapable of dealing with the phonon effect and also the quantum effect. Results show that regardless of the size of the graphene sheets applied, these published theoretical data, in particular, at temperatures below the Debye temperature (i.e., around 500-1000K for graphene/graphite [Hu, Ruan, Jiang, and Chen, 2009], these theoretical results all produce a smaller shear modulus than the present calculations and even the experimental results [Liu, Metcalf, Robinson, Houston, and Scarpa (2012)], once again suggesting that without considering the phonon effects in simulation, the shear and Young's modulus of graphene sheets would be underestimated.

3.3 Poisson's ratio

The calculated Poisson's ratios of the zigzag and armchair graphene sheets versus temperature in the range of 100-1500K and side length L of the square graphene sheets from 20-50 Å are presented in Fig. 8 and 9, respectively. It is shown that even though the increase of temperature would slightly decrease the Poisson's ratio, temperature in the range of 100-1500K would essentially have a little impact on the Poisson's ratio. On the other hand, there is a much more significant size effect on the Poisson's ratio, as compared to the temperature effect. The trend of the results is similar to that of the Young's and shear modulus aforementioned. As the side length increases from 20 to 50 Å, the Poisson's ratio at 300K is decreased from 0.245 to 0.170 for the zigzag of the graphene sheets and from 0.267 to 0.198 for the armchair. The reduction could be as much as about 30% in the side length range. Likewise, the Poisson's ratio tends to converge to a stable value (i.e., bulk Poisson's ratio) as the side length of the graphene sheets approaches 50 Å, where the bulk Poisson's ratios for the zigzag and armchair graphene sheets are 0.170 and 0.198, respectively.

The present calculation results are also compared with several literature theoret-

ical data [Reddy, Rajendran, and Liew (2006); Faccio, Denis, Pardo, Goyenola, and Mombro (2009); Min and Aluru (2011)], which are also shown in the figures. Specifically, for the zigzag type of graphene sheets, the literature data include [Reddy, Rajendran, and Liew (2006)] using the molecular statics, [Min and Aluru (2011)] using the standard NH thermostat incorporated with MD simulation and [Faccio, Denis, Pardo, Goyenola, and Mombro (2009)] using first-principles calculations with a periodic boundary condition assumption (i.e., considered as a bulk size). The respective sizes of the graphene sheets used in their calculations are $15.62 \times 17.22 \text{ \AA}^2$, $24.15 \times 17.22 \text{ \AA}^2$ and bulk size. In other words, the results of [Faccio, Denis, Pardo, Goyenola, and Mombro (2009)] could be regarded as a bulk Poisson's ratio. The size of the graphene sheet used in [Faccio, Denis, Pardo, Goyenola, and Mombro (2009)] is certainly not comparable to that of the present investigation, ranging from 20×20 to $50 \times 50 \text{ \AA}^2$. But the bulk value obtained from [Faccio, Denis, Pardo, Goyenola, and Mombro (2009)] can be used for comparison of the converged value of the Poisson's ratio as a function of the graphene sheet size. It is also important to note that these theoretical approaches lack account of the phonon effect. First of all, the results show that the converged value of the Poisson's ratio at 0K obtained from the present calculations is closely consistent with that of [Faccio, Denis, Pardo, Goyenola, and Mombro (2009)] at 0K. Moreover, Fig. 8 also shows that the calculation results at 300K for the $20 \times 20 \text{ \AA}^2$ graphene sheet size would be very comparable to that of [Reddy, Rajendran, and Liew (2006)] at 300K. However, the graphene sheet used in [Reddy, Rajendran, and Liew (2006)] (i.e., $15.62 \times 17.22 \text{ \AA}^2$) has a smaller size (area) than that of the present study. Thus, under the same graphene sheet size (or area), the predicted Poisson's ratio by [Reddy, Rajendran, and Liew (2006)] would be somewhat smaller than the present result according to the observed size-dependent trend of the Poisson's ratio. In addition, the presently calculated Poisson's ratio at 300K for the $20 \times 20 \text{ \AA}^2$ graphene sheet size match well with that of [Min and Aluru (2011)] at the same temperature and under a comparable graphene sheet size (area) (i.e., $24.15 \times 17.22 \text{ \AA}^2$), suggesting that the neglect of the phonon effect in the standard NH thermostat would have a little impact on the Poisson's ratio of graphene sheets at the temperature.

For the armchair type of graphene sheets, the published theoretical data by [Min and Aluru (2011)] using the standard NH thermostat at different graphene sheet sizes (or areas) are employed for comparison. The sizes of graphene sheets include 24.15×17.22 , 28.41×30.75 and $36.93 \times 38.13 \text{ \AA}^2$. Similar to the zigzag graphene sheets, temperature and size would reduce the Poisson's ratio, and size would hold a much more significant effect on the Poisson's ratio than temperature. Unsurprisingly, the calculation results of [Min and Aluru (2011)] also reveal the strong size

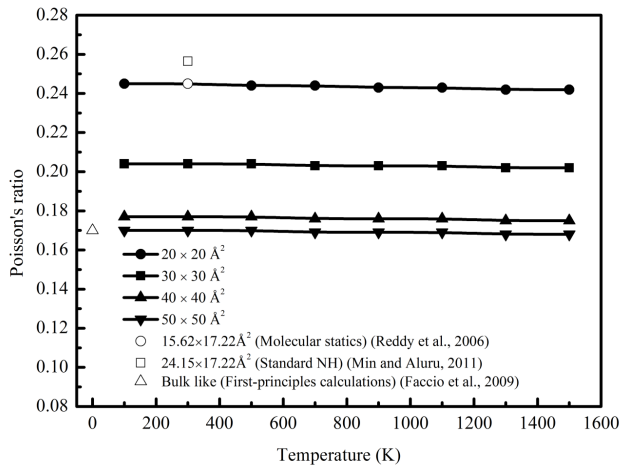


Figure 8: Poisson's ratio of zigzag graphene sheet as a function of temperature for various side lengths

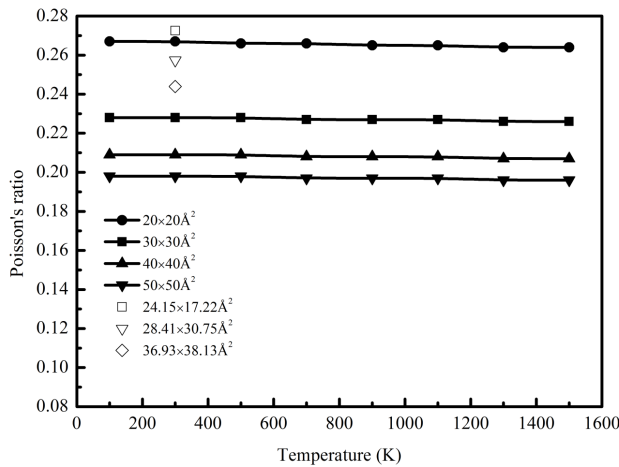


Figure 9: Poisson's ratio of armchair graphene sheet as a function of temperature for various side lengths

dependence of the Poisson's ratio. It is also evident to see that there is an acceptable agreement between the literature data using the standard NH thermostat and the present calculation results using the modified NH thermostat.

3.4 Specific heat of graphene sheet

The influences of temperature and size (area) on the specific heat (C_v) of the graphene sheets are shown in Fig. 10. Surprisingly, unlike the Young's modulus, and shear modulus and Poisson's ratio, the size of graphene sheets has a very little impact on the specific heat. The specific heat of the graphene sheet with area $50 \times 50 \text{ \AA}^2$ is further calculated using the standard NH, NHC, MNHC and velocity-rescaling thermostat incorporated with MD simulation, which lack account of the phonon effect and so the quantum effect, and these calculations are further compared with the theoretical data of [Jiang, Huang, and Hwang (2005)] using an ECM model with local harmonic approximation, which also takes into account the phonon effect, [Kittel (1996)] using the Debye theory, [Billings and Gray (1972)] using the experimental data and also the present calculations using the modified NH thermostat incorporated with MD simulation, as shown in Fig 11.

According to the Debye theory [Kittel (1996)], the specific heat will follow the T^3 -law at temperatures below the Debye temperature (i.e., around 500-1000K for graphene/graphite [Hu, Ruan, Jiang, and Chen (2009)]), where the specific heat of a solid at constant volume would vary with the cubic power of temperature. It is evident that without considering the phonon effect, just as the standard NH, NHC, MNHC and velocity-rescaling thermostat without a quantum correction, the predicted specific heats fail to present temperature independence, not to mention the well-known T^3 -law, suggesting that these thermostats are unable to yield an effective result. In other words, the modified NH thermostat is the only one among the five thermostats under comparison (i.e., the standard NH, NHC, MNHC, velocity-rescaling and modified NH thermostat) that can reproduce the well-known T^3 -relationship of the phonon low temperature specific heat. Most importantly, compared to the ECM model with local harmonic approximation that also accounts for the phonon effect, and even the experiment, the modified NH thermostat still provides a better prediction of the T^3 -law.

On the other hand, the specific heat obtained from the modified NH thermostat would approach a stable (converged) value at temperatures far above the Debye temperature. The result trend is also very consistent with those of [Jiang, Huang, and Hwang (2005); Kittel (1996); Billings and Gray (1972)]. Besides, for the results above the Debye temperature, the calculated specific heats by the standard NH, NHC, MNHC and velocity-rescaling thermostat are larger than the present calculation and also those of [Jiang, Huang, and Hwang (2005); Kittel, (1996);

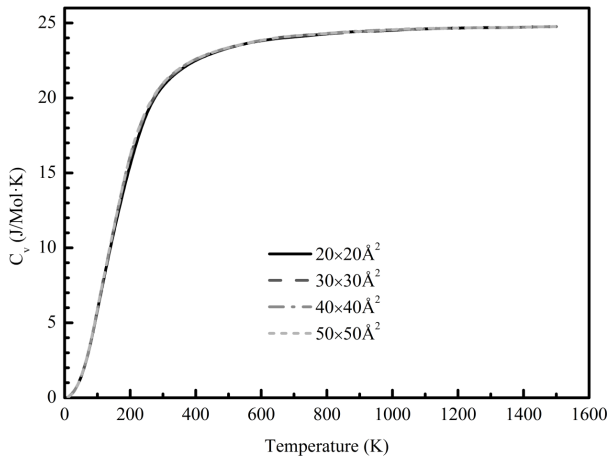


Figure 10: Specific heat (C_v) of graphene sheets as a function of temperature and under various side lengths

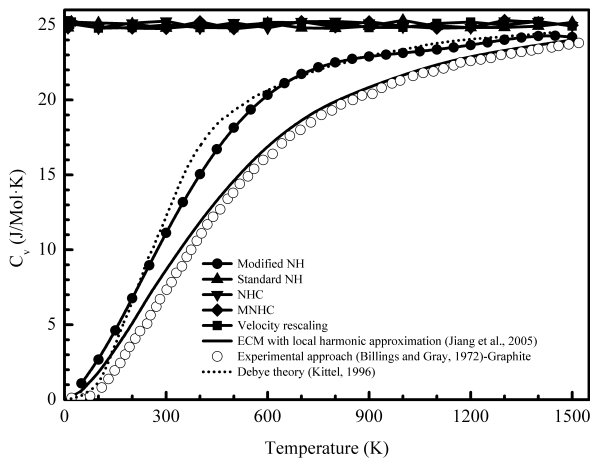


Figure 11: Predicted specific heats of a $50 \times 50 \text{ \AA}^2$ graphene sheet using the modified NH, standard NH, NHC, MNHC and velocity rescaling thermostats together with the literature theoretical and experimental data

Billings and Gray (1972)]. The tendency can be also observed in the temperature-dependent thermal conductivity of a short single-walled carbon nanotube predicted by [Cheng, Wu, and Chen (2012)]. Moreover, the present calculation is found to yield the most comparable result (i.e., 24.19 J/mol·K at 1500K) to the theoretical data obtained from the Debye theory and also the bulk specific heat value at the temperature (i.e., 23.80 J/mol·K) [Billings and Grey (1972)].

3.5 Linear and volumetric CTEs of graphene sheets

Figure 12 presents two different definitions of line change ratio ($\Delta L/L$). The first definition (i.e., definition 1) of line change ratio is obtained from the true length whereas the line change ratio that satisfies definition 2 is derived from the projected length of true length. Figure 13 plots the predicted linear CTE of a $50 \times 50 \text{ \AA}^2$ graphene sheet as a function a temperature based on these two line-change-ratio definitions. First of all, the predicted linear CTE of the graphene sheet consistent with definition 1 is unsurprisingly positive throughout the temperature range, and the CTE increases dramatically with temperature and eventually reaches a converged or stable value at temperatures approximately above 500K. The converged CTE value is about 6 ppm/K. By contrast, the calculated linear CTE of the graphene sheet that is based on definition 2 is negative at temperatures below approximately 293 K, and at temperatures above, similar to definition 1, it significantly increases with temperature and also approach a converged or stable value at temperatures above 1500K. In general, most materials have positive CTE, and they would expand when heated while contract as cooled. An exception to the rule is a membrane, which often has a negative CTE. This particular phenomenon may arise from the very soft out-of-plane acoustic phonon mode in the 2D membranes, which, contrary to acoustic phonons in the most materials, increases in frequency when inter-atomic spacing is increased [Lau, Bao, and Velasco (2012)]. A negative in-plane CTE in many layered compounds, including graphene, may result from such “membrane effect”, first reported by [Lifshitz (1952)].

The theoretical data [Jiang, Huang, and Hwang (2005); Jiang, Wang, and Li (2009b)] concerning the linear CTE of a graphene sheet and the experimental data for the linear CTE of graphite [Billings and Grey (1972); Pierson (1993)] are also adopted for comparison, as displayed in Fig. 13. In the theoretical works, including [Jiang, Huang, and Hwang (2005)] using an ECM model with local harmonic approximation, applied a periodic boundary condition in their calculations. The results in Fig. 13 clearly demonstrate that the predicted CTE of the graphene sheet agrees reasonably with the data of [Jiang, Huang, and Hwang (2005)] using an ECM model with the local harmonic approximation throughout the temperature range. It is further observed that the negative CTE of [Jiang, Huang, and Hwang (2005)] is in

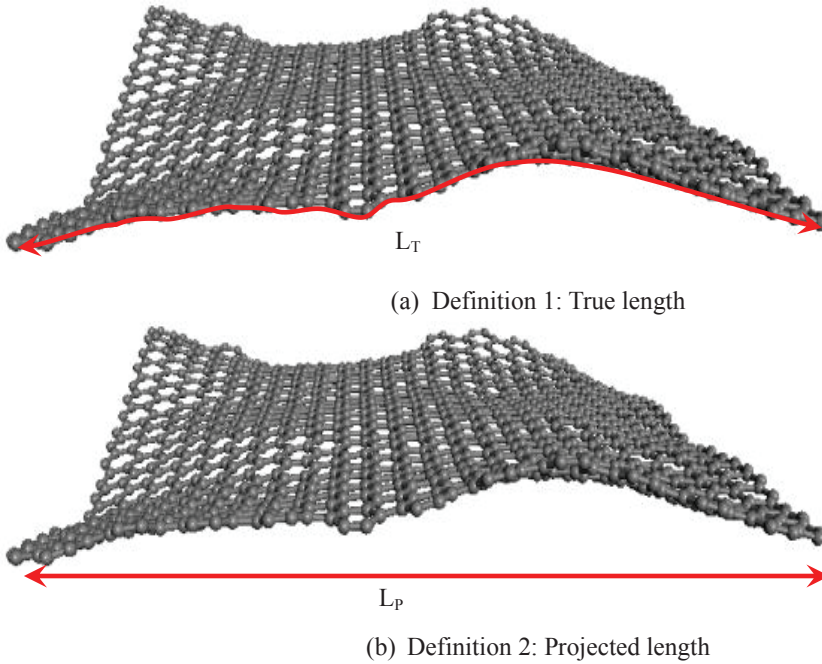


Figure 12: Two definitions of line change ratio ($\Delta L/L$)

the range of 0 to 456K, which is consistent with that of the present results (i.e., around 0 to 500K). Likewise, a good consistency can be also observed between the calculated CTE of graphene sheet and the experimental value for graphite [Billings and Grey (1972); Pierson (1993)] as the temperature is less than 200K. However, a clear discrepancy exists between the calculated CTE of graphene sheet and the experimental value for graphite when the temperature is up to about 200K.

Generally, the volumetric CTE is three times the linear CTE for an isotropic material. However, a graphene sheet is highly anisotropic. Accordingly, its volumetric CTE cannot be obtained simply by multiplying its linear CTE by three. In this study, the atoms in the graphene sheet vibrate as the temperature is varied, resulting in a deformed graphene sheet with an irregular shape. Besides, the graphene sheet would also deform at a free relaxation state simply because the surface effect.

In general, it is not straightforward to determine the volume of a highly deformed graphene sheet. Rather, to estimate the volume of the deformed graphene sheet, the Connolly surface method [Connolly (1993)] is utilized in the study. The Connolly surface is widely regarded as a useful approach for estimating molecular surface

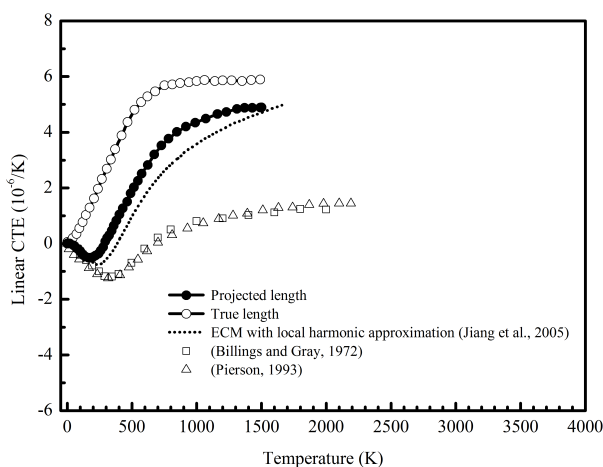


Figure 13: CTE of $50 \times 50 \text{ \AA}^2$ graphene sheet as a function of temperature

[Cao, Pham, Tonge, and Nicolau (2002); Decherchi, Colmenares, Catalano, Spagnuolo, Alexov, and Rocchia (2013)]. Figure 14 schematically depicts the imaginary volume of the graphene sheet through the Connolly surface method. The volumetric CTE of the graphene sheets at different side lengths calculated by the modified NH thermostat is plotted against temperature, as shown in Fig. 15. It is found that similar to the linear CTE of the graphene sheets that is based on definition 1, as shown in Fig. 12, the volumetric CTE would also reveal a high dependence on temperature at low temperatures or temperatures below the Debye temperature, and similar to the specific heat, the volumetric CTE does not seem to depend on the size of the graphene sheets. Then, It would also converge to a limit at high temperature or temperatures far above the Debye temperature, and the approximate limits for the 20×20 , 30×30 , 40×40 and $50 \times 50 \text{ \AA}^2$ graphene sheets at 1500 K are 14.12×10^{-6} , 14.22×10^{-6} , 14.34×10^{-6} and $14.42 \times 10^{-6} \text{ 1/K}$. It is clear to see that the limit would slightly increase with an increasing size, and the trend of the result is also consistent with that of the linear CTE.

In addition to the modified NH thermostat, the volumetric CTE of the $50 \times 50 \text{ \AA}^2$ graphene sheet at different temperatures are also calculated using the standard NH, NHC, MNHC and velocity-rescaling thermostat. Similar to the specific heat presented in Fig. 11, the standard NH, MNHC and NHC thermostats still fail to demonstrate the power-law dependence of the CTE on temperature at low temperatures or temperatures below the Debye temperature. Likewise, they remain a

constant value throughout the temperature range. Again, the modified NH thermostat is the only one among the five thermostats under comparison that can give the power-law temperature dependence of the volumetric CTE.

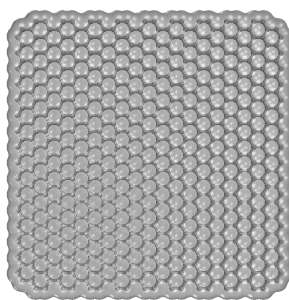


Figure 14: Imaginary volume of graphene sheet by Connolly surface method

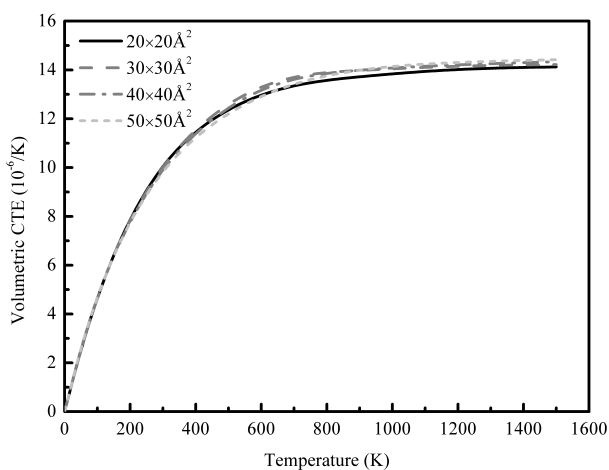


Figure 15: Volumetric CTE of graphene sheets at different side lengths as a function of temperature

4 Conclusions

Because of the benefits of reducing the high fluctuation of the instantaneous system temperature that is calculated by the standard NH thermostat method and avoidance of an underestimate of the system temperature, the modified NH thermostat method is applied herein in a constant-temperature MD simulation to examine the temperature-dependent Young's modulus, shear modulus, Poisson's ratio, linear and volumetric CTEs and specific heat of zigzag and armchair graphene sheets in a square shape. Their size dependences are also investigated. The calculated results are compared with those obtained using the standard NH, NHC, MNHC and velocity rescaling thermostat and also with the literature experimental and theoretical data.

Some concluding remarks are drawn:

1. It turns out that the calculated thermal-mechanical and thermodynamic results of the graphene sheets at different side lengths and temperatures using the modified NH thermostat would have a better agreement with the published experimental data as compared to other theoretical approaches and the other four existing thermostats, namely the standard NH, NHC, MNHC and velocity rescaling.
2. The calculations demonstrate that the Young's modulus, shear modulus and Poisson's ratio of the zigzag and armchair graphene sheets would decrease as the temperature and side length of graphene sheets increase whereas the linear and volumetric CTEs and specific heat vary slightly with an increasing side length.
3. It is shown that the size (side length) would have a larger impact on the mechanical properties of graphene sheets than the temperature. However, the volumetric CTE and specific heat of graphene sheets vary slightly as the side length increases from 20 Å to 50 Å, revealing that the size has a little effect on them.
4. The Young's and shear modulus and the Poisson's ratio of the zigzag and armchair graphene sheets would converge to a stable value when the side length reaches approximately 40 Å and over 50 Å, respectively. The converged results reveal that the armchair graphene sheet tends to hold a larger Young's and shear modulus and Poisson's ratio than the zigzag one.
5. The modified NH is the only one among the five thermostats for comparison that can accurately reproduce the Debye T^3 -law of the phonon low temper-

ature specific heat and also the power-law temperature dependence of the linear and volumetric CTEs of graphene sheets.

6. The calculated linear CTE of graphene sheets would be strongly dependent on the line-change-ratio assumptions. The predicted linear CTE of the graphene sheet under the definition of the line change ratio that is derived from the projected length of true length would have a negative value in the temperature range of 0-293K, perhaps owing to the membrane effect.
7. The predicted volumetric CTE and specific heat of the graphene sheets shows a converged, stable value at high temperatures or temperatures far above the Debye temperature.

Acknowledgement

The authors would like to thank the National Science Council of the Republic of China, Taiwan, for financial support of this research under Contract No. NSC101-2221-E-007-009-MY3 and NSC100-2221-E-035-036-MY3.

References

- Billings, B. H.; Gray, D. E.** (1972): American Institute of Physics Handbook, McGraw-Hill, New York.
- Bunch, J. S.; van der Zande, A. M.; Verbridge, S. S.; Frank, I. W.; Tanenbaum, D. M.; Parpia, J. M.; Craighead, H. G.; McEuen, P. L.** (2007): Electromechanical Resonators from Graphene Sheets. *Science*, vol. 315, pp. 490–493.
- Cammarata, R. C.; Sieradzki, K.** (1989): Effects of surface stress on the elastic moduli of thin films and superlattices. *Physical Review Letters*, vol. 62, pp. 2005–2008.
- Cao, J.; Pham, D. K.; Tonge, L.; Nicolau, D. V.** (2002): Predicting surface properties of proteins on the Connolly molecular surface. *Smart Materials and Structures*, vol. 11, pp. 772–777.
- Chen, W. H.; Cheng, H. C.; Hsu, Y. C.** (2007): Mechanical Properties of Carbon Nanotubes Using Molecular Dynamics Simulations with the Inlayer van der Waals Interactions. *Computer Modeling in Engineering & Sciences*, vol. 20, pp. 123–145.
- Cheng, H. C.; Liu, Y.-L.; Chen, W. H.** (2009): Atomistic-Continuum Modeling for Mechanical Properties of Single-Walled Carbon Nanotubes. *International Journal of Solids and Structures*, vol. 46, pp. 1695-1704.

- Chen, W. H.; Wu, C. H.; Cheng, H. C.** (2011a): Modified Nosé–Hoover Thermostat for Solid State for Constant Temperature Molecular Dynamics Simulation. *Journal of Computational Physics*, vol. 230, pp. 6354–6366.
- Chen, W. H.; Wu, C. H.; Cheng, H. C.** (2011b): Temperature-dependent Thermodynamic Behaviors of Carbon Fullerene Molecules at Atmospheric Pressure. *Computers, Materials, & Continua*, vol. 25, No. 3, pp. 195–214.
- Chen, W. H.; Liu, Y. L.; Wu, C. H.; Cheng, H. C.** (2012): A Theoretical Investigation of Thermal Effects on Vibrational Behaviors of Single-Walled Carbon Nanotubes. *Computational Materials Science*, pp. 226–233
- Cheng, H. C.; Hsu, Y. C.; Chen, W. H.** (2009): The Influence of Structural Defect on Mechanical Properties and Fracture Behaviors of Carbon Nanotubes. *Computers, Materials, & Continua*, vol. 11, pp. 127–146.
- Cheng, H. C.; Chen, W. H.; Wu, C. H.** (2012): Low Temperature Thermal Conductivity of Short Single-Wall Carbon Nanotubes Using a Modified Nosé–Hoover Thermostat. *Nanoscale and Microscale Thermophysical Engineering*, vol. 16, pp. 242–259.
- Connolly, M. L.** (1993): The molecular surface package. *Journal of Molecular Graphics*, vol. 11, no. 2, pp. 139–141.
- Cranford, S.; Buehler, M. J.** (2011): Twisted and coiled ultralong multilayer graphene Ribbons. *Modelling and Simulation in Materials Science and Engineering*, vol. 19, pp. 054003(1)–054003(20).
- Debye, P.** (1912): Zur Theorie der spezifischen Waerme. *Annalen der Physik (Leipzig)*, vol. 39, pp. 789–839.
- Decherchi, S.; Colmenares, J.; Catalano, C. E.; Spagnuolo, M.; Alexov, E.; Rocchia, W.** (2013): Between algorithm and model: different Molecular Surface definitions for the Poisson-Boltzmann based electrostatic characterization of biomolecules in solution. *Communications in Computational Physics*, vol. 13, pp. 61–89.
- Dingreville, R.; Qu, J.** (2005): Surface free energy and its effect on the Young’s behavior of nano-sized particles, wires and films. *Journal of the Mechanics and Physics of Solids*, vol. 53, pp. 1827–1854.
- Erkoc, S.** (1997): Empirical many-body potential energy function used in computer simulations of condensed matter properties. *Physics Reports*, vol. 278, pp.79–105.
- Faccio, R.; Denis, P.; Pardo, H.; Goyenola, C.; Mombru, A. W.** (2009): Mechanical properties of graphene nanoribbons. *Journal of Physics-Condensed Matter*, vol. 21, no. 2, pp. 285304.
- Fukushima, H.; Drzal, L. T.** (2002): Graphite nanoplatelets as reinforcements for

polymers: structural and electrical properties. In: Proceedings of the American society for composites, *the 17th technical conference*, pp. 21–23.

Geim, A. K.; Novoselov, K. S. (2007): The rise of graphene. *Nature Materials*, vol. 6, pp. 183–191.

Gonze, X.; Beuken, J. M.; Caracas, R.; Detraux, F.; Fuchs, M.; Rignanese, G. H.; Sindic, L.; Verstraete, M.; Zerah, G.; Jollet, F.; Terrent, M.; Roy, A.; Mikami, M.; Ghose, P.; Ratty, J. Y.; Allan, C. D. (2002): First-principles computation of material properties: the ABINIT software project. *Computational Materials Science*, vol. 25, pp. 478–492.

Guo, J. G.; Zhao, Y. P. (2005): The size-dependent Young's properties of nanofilms with surface effects. *Journal of Applied Physics*, vol. 98, pp. 074306.

Han, T.; He P.; Zheng, B. (2009): Dependence of the Tensile Behavior of Single Graphene Sheet on Temperature and Strain Rate. *17th International Conference on Composites or Nano Engineering*.

Hoover, W.G. (1985): Canonical Dynamics: Equilibrium Phase-Space Distributions, *Physical Review A*, vol. 31, pp. 1695–1697.

Hu, J.; Ruan, X.; Jiang, Z.; Chen, Y. P. (2009): Molecular Dynamics Calculation of Thermal Conductivity of Graphene Nanoribbons. *American Institute of Physics Conference Proceedings*, vol. 1173, pp. 135–138.

Inoue, Y.; Kobayashi, R.; Ogata, S.; Gotoh, T. (2010): Numerical simulation of fluid induced vibration of graphenes at micron scales. *Computer Modeling in Engineering & Sciences*, vol. 6, pp. 137–161.

Jiang, H.; Huang, Y.; Hwang, K. C. (2005): A Finite-Temperature Continuum Theory Based on Interatomic Potentials. *Transactions of the ASME*, vol. 127, pp. 408–416.

Jiang, J. W.; Wang, J. S.; Li, B. (2009a): Young's modulus of graphene: A molecular dynamics study. *Physical Review B*, vol. 80, pp. 113405(1)–113405(5).

Jiang, J. W.; Wang, J. S.; Li, B. (2009b): Thermal expansion in single-walled carbon nanotubes and graphene: Nonequilibrium Green's function approach. *Physical Review B*, vol. 80, pp. 205429(1)–205429(7).

Kim, K. S.; Zhao, Y.; Jang, H.; Lee, S. Y.; Kim, J. M.; Kim, K. S.; Ahn, J. H.; Kim, P.; Choi, J. Y.; Hong, B. H. (2009): Large-scale pattern growth of graphene films for stretchable transparent electrodes. *Nature*, vol. 457, pp. 706–710.

Kittel, C. (1996): Introduction to Solid State Physics 7th edition (John Wiley & Sons, New York).

Konstantinova, E.; Dantas, S. O.; Barone, P. M. V. B. (2006): Electronic and elastic properties of two-dimensional carbon planes. *Physical Review B*, vol. 74,

pp. 035417(1)–035417(6).

Li, C.; Chou, T. W. (2003): A structural mechanics approach for the analysis of carbon nanotubes. *International Journal of Solids and Structures*, vol. 40, pp. 2487–2499.

Lau, C. N.; Bao, W.; J. Jr., Velasco (2012): Properties of suspended graphene membranes. *Materials Today*, vol. 15, pp. 238–245.

Lifshitz, I. M. (1952): Thermal properties of chain and layered structures at low temperatures. *zh eksp teor fiz*, vol. 22, pp. 475–486.

Liu, X.; Metcalf, T. H.; Robinson, J. T.; Houston, B. H.; Scarpa, F. (2012): Shear Modulus of Monolayer Graphene Prepared by Chemical Vapor Deposition. *Nano Letters*, vol. 12, pp. 1013–1017.

Lee, C.; Wei, X.; Kysar, J. W.; Hone, J. (2008): Measurement of the Elastic Properties and Intrinsic Strength of Monolayer Graphene. *Science*, vol. 321, pp. 385–388.

Martyna, G. J.; Tuckerman, M. E.; Klein, M. L. (1992): Nosé–Hoover chains: The canonical ensemble via continuous dynamics. *Journal of Chemical Physics*, vol. 97, pp. 2635–2643.

Mounet, N.; Marzari, N. (2005): First-principles determination of the structural, vibrational and thermodynamic properties of diamond, graphite, and derivatives. *Physical Review B*, vol. 71, p. 205214.

Meyer, J. C.; Geim, A. K.; Katsnelson, M. I.; Novoselov, K. S.; Booth, T. J.; Roth, S. (2006): The structure of suspended graphene sheets. *Nature*, vol. 446, pp. 60–63.

Min, K.; Aluru, N. R. (2011): Mechanical properties of graphene under shear deformation. *Applied Physics Letters*, vol. 98, p. 013113.

Mohanty, N.; Berry, V. (2008): Graphene-based single-bacterium resolution biodevice and DNA transistor: interfacing graphene derivatives with nanoscale and microscale biocomponents. *Nano Letters*, vol. 8, pp. 4469–4476.

Nosé, S. (1984): A Molecular Dynamics Method for Simulations in the Canonical Ensemble. *Molecular Physics*, vol. 52, pp. 255–268.

Novoselov, K. S.; Geim, A. K.; Morozov, S. V.; Jiang, D.; Zhang, Y.; Dubonos, S. V.; Grigorieva, I. V.; Firsov, A. A. (2004): Electric Field Effect in Atomically Thin Carbon Films. *Science*, vol. 306, pp. 666–669.

Novoselov, K. S.; Jiang, D.; Schedin, F.; Booth, T. J.; Khotkevich, V. V.; Morozov, S. V. (2005): Two-dimensional atomic crystals. *Proceedings of the National Academy of Sciences*, vol. 102, pp. 0451–0453.

- Odegard, G. M.; Gates, T. S.; Nicholson, L. M.; Wise, K. E.** (2002): Equivalent-continuum modeling of nano-structured materials. *Composites Science and Technology*, vol. 62, pp. 1869–1880.
- Pierson, H. O.** (1993): Handbook of Carbon, Graphite, Diamond, and Fullerenes: Properties, Processing, and Applications (Noyes Publications, Park Ridge, NJ) pp. 59–60.
- Popov, V. N.; Van Doren, V. E.; Balkanski, M.** (2000): Elastic properties of single-walled carbon nanotubes. *Physical Review B*, vol. 61, pp.3078–3084.
- Pozrikidis, C.** (2008): Mechanics of hexagonal atomic lattices. *International Journal of Solids and Structures*, vol. 45, pp. 732–745.
- Reddy, C. D.; Rajendran, S.; Liew, K. M.** (2006): Equilibrium configuration and continuum elastic properties of finite sized graphene. *Nanotechnology*, vol. 17, pp. 864–870.
- Sakhaee-Pour, A.** (2009): Elastic properties of single-layered graphene sheet. *Solid State Communications*, vol. 149, pp. 91–95.
- Shi, G.; Zhao, P.** (2011): A New Molecular Structural Mechanics Model for the Flexural Analysis of Monolayer Graphene. *Computer Modeling in Engineering & Sciences*, vol. 71, pp. 67–92.
- Stankovich, S.; Dikin, D. A.; Dommett, G. H. B.; Kohlhaas, K. M.; Zimney, E. J.; Stach, E. A.; Piner, R. D.; Nguyen, S. T.; Ruoff, R. S.** (2006a): Graphene-based composite materials. *Nature*, vol. 442, pp. 282–286.
- Stankovich, S.; Piner, R. D.; SonBinh, T. N.; Ruoff, R. S.** (2006b): Synthesis and exfoliation of isocyanate-treated graphene oxide nanoplatelets. *Carbon*, vol. 15, pp. 3342–3347.
- Wei, T.; Luo, G. L.; Fan, Z. J.; Zheng, C.; Yan, J.; Yao, C. Z.; Li, W. F.; Zhang, C.** (2009): Preparation of graphene nanosheet/polymer composites using in situ reduction–extractive dispersion. *Carbon*, vol. 47, pp. 2296–2299.
- Woodcock, L.V.** (1971): Isothermal Molecular Dynamics Calculations for Liquid Salts. *Chemical Physics Letters*, vol. 10, pp. 257–261.
- Yi, L. J.; Chang, T. C.** (2012): Loading direction dependent mechanical behavior of graphene under shear strain. *Physics, Mechanics & Astronomy*, vol. 55, pp. 1083–1087.

